Proceedings World Geothermal Congress 2026
Calgary, Canada, June 8 – 11, 2026

The Relative Moment Tensor Method to Characterize EGS Reservoirs Using Induced Seismicity - A Case Study from the Helsinki (Finland) EGS Experiment

Wasja Bloch[1]*, Volker Oye[1], Doriane Drolet[2], Michael G. Bostock[3], Alexandre Plourde[4], and Grzegorz Kwiatek[5]
NORSAR[1]*, Carbon Management Canada[2], The University of British Columbia[3] , Natural Resources Canada[4], GMuG GmbH[5]
wasja@norsar.no

Keywords: EGS, Induced Seismicity, Moment Tensor, Fracture network, Stimulation

INTRODUCTION

The development of Enhanced Geothermal Systems (EGS) is gaining momentum as demand for reliable and emission-free power and heat sources rises and drilling technologies for igneous and hot rocks advance. "Enhancement" of the geothermal system refers to the process of hydraulic stimulation, where water is pumped into the target formation to open subsurface fractures, increasing permeability and facilitating the fluid circulation that transports heat from the reservoir to the surface. Reservoir stimulation can in some cases pose risks, as induced seismicity may agitate nearby population and industry. The possible triggering of tectonic earthquakes by stimulation fluids is a rare, but severe complication. At the same time, the properties of the induced seismicity hold valuable engineering information for example about the activated fracture network or the subsurface pressure distribution. Specifically, the seismic moment tensor (MT) yields a description of the size and orientation of a single activated fracture. Large MT datasets are useful to characterize flow capacities and provide means to optimize field production. While the computation of *absolute* MTs by waveform inversion is data intensive and can be performed only for larger events, *relative* MTs rely on less subsurface information and may be computed for small seismic events.

We here introduce *relMT*, a research-grade software package to compute relative earthquake moment tensors. We showcase the application of *relMT* to the EGS hydraulic stimulation performed within the St1 Deep Heat project in the Helsinki metropolitan area, Finland (Fig. 1). A total of 18,500 m^3 water was injected into gneisses and granites of the Fennoscandian Shield at a depth of 6,100 m. Induced seismicity was monitored using 12 3-component geophones in shallow boreholes and one geophone chain at ~2 km depth, of which we used 10 surface stations for our analysis. A total of 1,968 seismic events could be re-located with precision, down to magnitude -0.5 (Leonhardt et al., 2021). Of these events, we are able to compute 823 relative moment tensors.

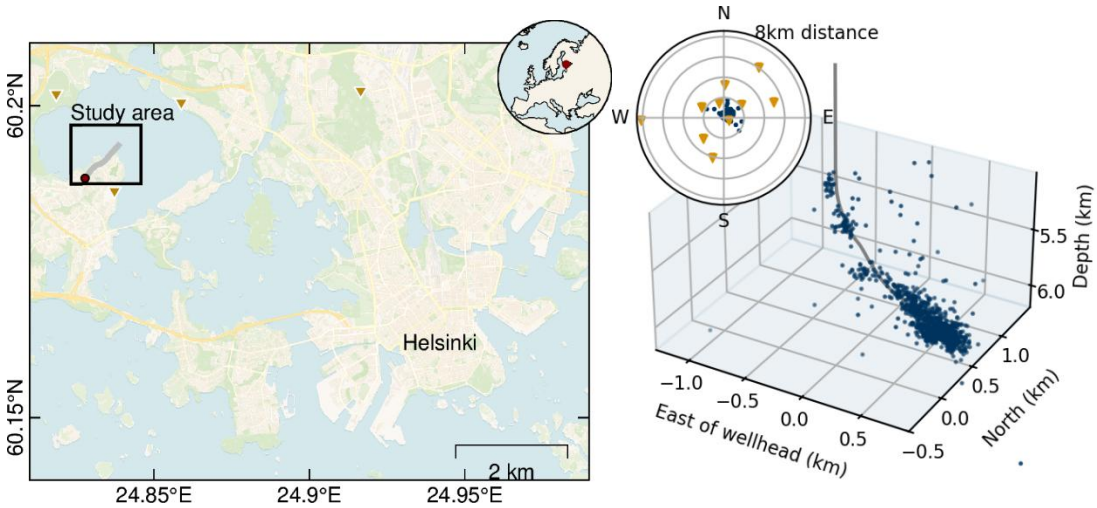


Figure 1. Overview over study area. Left: Location map of the in the Helsinki metropolitan area. Right: Seismic event cloud of the 2018 stimulation of the geothermal OTN-3 well in Espoo near Helsinki, Finland. The 1,968 relocated events from Leonhardt et al. (2021) are shown. Inset map shows azimuth and distance of the seismic monitoring network. Borehole trajectory in gray, seismic stations as inverted yellow triangles. Background map tiles © OpenStreetMap contributors © CARTO

1 METHOD

We computed relative moment tensors following the approach of Plourde and Bostock (2019). The method assumes similar Green's functions for closely spaced seismic events and a point approximation of the seismic source. Under these assumptions, the relative amplitude between seismograms can be attributed to the difference in moment tensor between the events. Compared to absolute methods, path and site effects cancel out when computing relative moment tensors and so do not need to be considered.

In synopsis, we measure amplitude ratios between seismic events on single seismic stations. The relative amplitudes are combined mathematically with ray take-off angles, relative event locations and one absolute reference moment tensor in a linear system of equations. The solution of the linear system with algebraic methods yields the relative moment tensors of all events connected by relative amplitude measurements. The uncertainty of the solutions is quantified using the bootstrap method.

We implemented the methodology in the open-source software package *relMT* (Bloch et al., 2026). The software takes as inputs seismic waveforms stored as *NumPy* arrays, event locations, ray take-off angles, and reference MTs stored as text files, as well as waveform headers and a configuration file. It then provides methods to align the waveforms, to exclude uncertain measurements, to measure the relative amplitudes, to control the quality of the amplitude measurements, to solve the linear system and to compute uncertainty estimates. It is under active development on GitHub (https://github.com/wasjabloch/relmt).

1.1 Waveform Alignment

For the Helsinki stimulation dataset, we aligned waveforms in a two-step procedure. In the first step, we selected relatively wide, 0.3 second time windows around the analyst time picks, and pre-aligned the waveforms in the 1-40 Hz band. After that, we selected shorter time windows between 0.04 and 0.2 seconds length, specific to each phase observation, and repeated the alignment procedure. To reduce computational cost, we combined each event only with its 200 nearest neighbours when aligning S-waves.

In each alignment iteration, we computed pair- and triplet-wise cross-correlation lag times for P- and S-waves, respectively. We honoured possible polarity reversals for P-waves and planar polarization of S-waves by formulating appropriate objective functions. The time lags were then inverted for optimal time shifts per event wave train. Alignment was refined to sub-sample accuracy by regarding each seismogram section as a matrix and maximizing the energy that is projected onto the first principal component of that matrix for P-waves, or onto the first *two* principal components for S-waves (Bostock et al. 2021).

1.2 Relative amplitude measurement and quality control

We measured relative amplitudes automatically from the waveform sections. For each event, an optimal high- and lowpass filter corner was determined automatically for which the signal-noise-ratio was greater than 0 dB within the passband and the lowpass frequency was below the apparent corner frequency of the event, so as to satisfy the point-source assumption. Relative amplitudes were measured on the passband that contained the frequency range of all contributing events (2 for P-waves and 3 for S-waves), with a dynamic range of at least 2 dB.

Relative amplitudes were measured as the ratios of the expansion coefficients of the singular value decomposition of the waveform matrix $G = U\Sigma V^T$. For the P-waves of events *a* and *b* the amplitude ratio is $A_{ab} = V_{a1}/V_{b1}$. For S-waves, a third waveform *c* is required to account for planar polarization. The relative amplitudes B_{abc} and B_{acb} to reconstruct event *a* from *b* and *c* are retrieved from the system: $\mathrm{V_{b1}B_{abc} + V_{c1}B_{acb} = V_{a1}}$, and $\mathrm{V_{b2}B_{abc} + V_{c2}B_{acb} = V_{a2}}$ (Plourde and Bostock, 2019).

The quality of the amplitude measure is quantified via the normalized amplitude reconstruction misfit $\mu = \frac{|\boldsymbol{u}` - \boldsymbol{u}|}{|\boldsymbol{u}|}$ where $\boldsymbol{u}$ and $\boldsymbol{u}'$ denote the observed and reconstructed seismogram waveforms, respectively, and $|\boldsymbol{u}|$ denotes the vector norm of $\boldsymbol{u}$. We excluded waveform reconstructions with a misfit larger than 0.2 for P-waves and 0.4 for S-waves, resulting in ~170k relative P- and ~13M relative S-amplitude measurements. Events with an azimuthal gap larger than 270° or less than 10 equations were discarded. To reduce redundancy in S-amplitude measurements, we ranked the remaining observations: 1. by the number of occurrences of the events of the triplet in the observation set, 2. the total count of the station the observation was made on, and 3. by the normalized amplitude misfit μ. We then iteratively discard the top 1% of the so defined most redundant observations until we reach a threshold of 1M S-measurements. At this threshold, solution of the linear system takes about one minute on our desktop workstation.

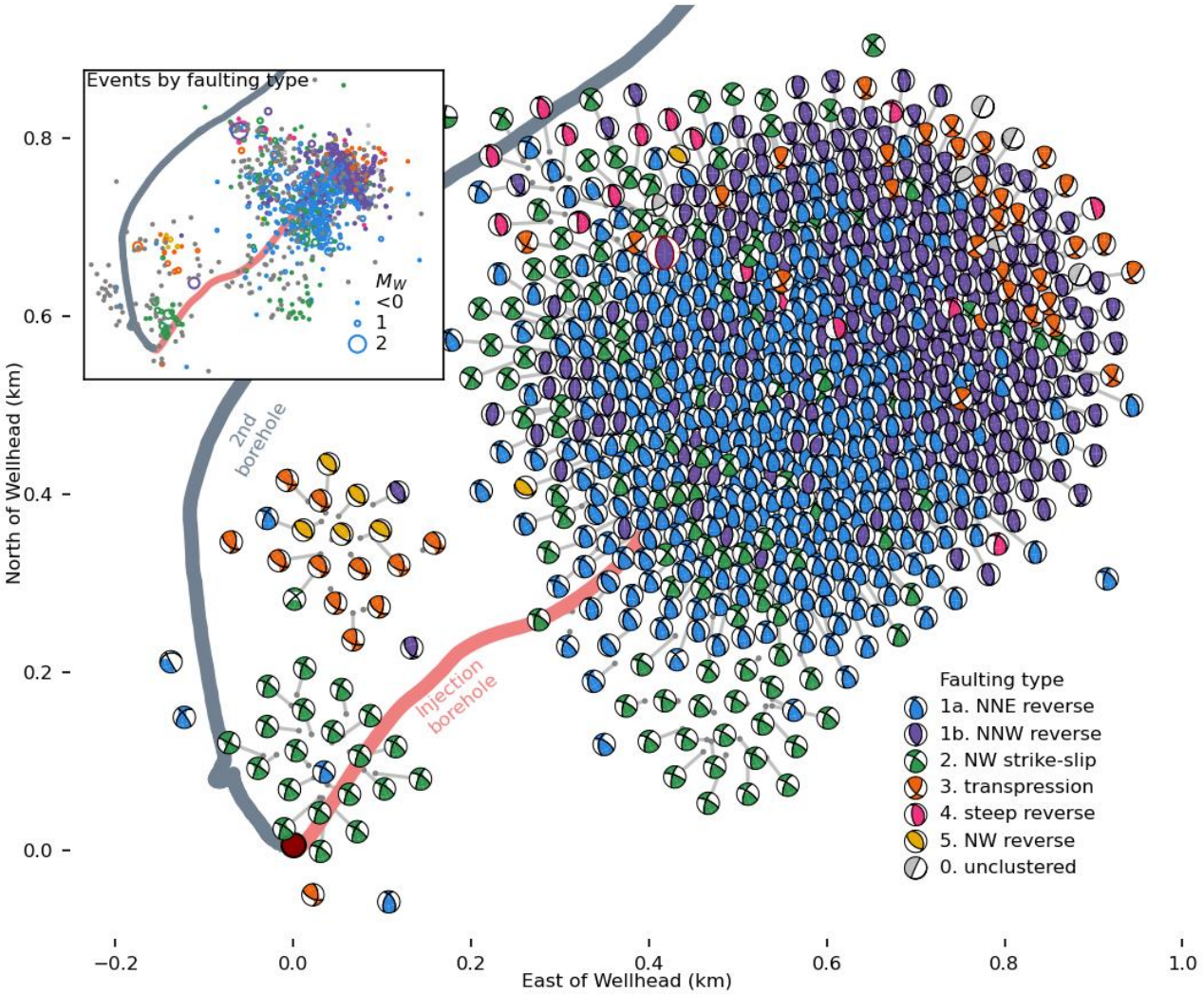


Figure 2. Map view of the retrieved relative moment tensor solution. The reference event is plotted enlarged and with a red outline. Beachball plots are moved apart as to not overlap. Events are colored by faulting type. Inset: Same map extend, but no beachballs superimposed. Gray line marks the borehole trajectory.

1.3 Solution of the Linear System and Uncertainties

Following Plourde and Bostock (2019), we multiply the relative amplitudes by the polarization vectors derived from the ray take-off angles and set up the linear system of equations that relates the amplitude measurements to the relative moment tensors. We apply equation weights derived from the inverse maximum amplitude and μ. As a constraint to the linear system, we test each of the absolute moment tensors computed by Rintamäki et al. (2025). The comparison additionally serves us as a means to validate our results. We find the best agreement between results when using the 2018-06-11, 13:42 M0.5 reverse faulting event as a reference. We first computed full moment tensor solutions. From those, we excluded 147 outlying events with an isotropic component > 25% or a double-couple component < 25% and re-computed the results applying a deviatoric (non-isotropic) constraint.

2 RESULTS AND INTERPRETATION

We retrieved a total of 823 relative moment tensors down to M_W=-0.5, compared to previously 283 absolute MTs down to M_W=0.3 (Rintamäki et al., 2025). The misorientation between absolute and relative MTs in terms of the Kagan angle is $12°^{+14°}_{-5°}$ (median, 10%, 90% quantiles).

We clustered events within a Kagan angle deviation of 45° using the *Weighted Pair Group Method with Arithmetic Mean* (WPGMA) method. The clustering results in seven faulting type groups (Fig. 2): 1a. NNE-striking reverse (355 events), 1b. NNW-striking reverse (265 events), 2. NW-striking left-lateral strike-slip (131 events) 3. transpression (43 events), 4. steep reverse (16 events), 5. NW-striking reverse (7 events). The right-hand rule

applies for the relation between interpreted strike and dip direction. 6 events did not cluster in groups with at least 5 members. Groups 1, 2, and 3 were previously reported by Rintamäki et al. (2025).

Faulting is dominantly reverse with ~N-striking faults (group 1, Fig. 2), with a notable number of transpressional mechanisms (groups 2 and 3). The seismic event cloud exhibits NW-SE-oriented streaks. Stress field analysis suggests that the majority of the activated faults strike approximately N to NW and dip east (Rintamäki et al., 2025). Accordingly, we interpret the N(W)-S(E) striking planes of the focal mechanisms to be the fault plane, while the NE-SW-striking planes are more likely the auxiliary planes. This interpretation implies that the transform-faulting component is left-lateral and that subordinate groups (3, 4, and possibly 5) may rupture on conjugate, west-dipping faults.

The faulting types appear to be closely related to the spatial position of the events within the seismic event cloud. While the N-striking reverse faults (group 1) typically occur closer to the injection interval, transpressional mechanisms (groups 2 and 3) are located in the south-western and shallower part of the event cloud. Most notably, two isolated spatial clusters of seismicity occurred 300-500 m above the injection intervals, close to the borehole, around 100 and 300 m north of the wellhead, respectively. They yield characteristic faulting types of group 2 and group 3, respectively.

3 DISCUSSION

Kwiatek et al. (2019), report the local stress field for the investigated volume with the largest principal stress (σ_1) oriented horizontally N110°E and the lowest principal stress (σ_3) vertical. The reverse faulting events of group 1 appear to be close to optimally-oriented to this stress field. Conversely, faulting mechanisms with a significant strike-slip component (groups 2 and 3) or a strike close to σ_1 (group 5) may be misaligned with the stress field, suggesting that faulting is at least to some degree controlled structurally. Remarkably, group 1 events are typically located closer to the injection interval. Here, the highest fluid pressures may cause fracturing of pristine rock, irrespective of pre-existing structures. Fractures hosting events of the other groups may require a relatively lower fluid pressure to fail, suggesting the prevalence of pre-existing weakness zones of an orientation indicated by the focal mechanisms.

The abundance of focal mechanisms and relative moment magnitudes (M_W) delivered by the relative moment tensor method facilitates statistical analysis of faulting processes under consideration of the source mechanism. For example, the slope of the Gutenberg-Richter relationship (*b*-value) has been widely adopted in statistical seismology to characterize the seismogenic potential of the subsurface. When preliminarily investigating the magnitude distribution within the faulting-type groups, we find a tendency of larger events to be overrepresented in group 1, compared to all events combined (Fig. 3). This behavior may be due to the association of group 1 events with a more homogenously structured, potentially smoother fracture network, allowing them to grow bigger. Conversely, the potentially structurally-controlled fractures of group 2 may be more heterogenous, or rougher, with a conceivably smaller relative rupture area.

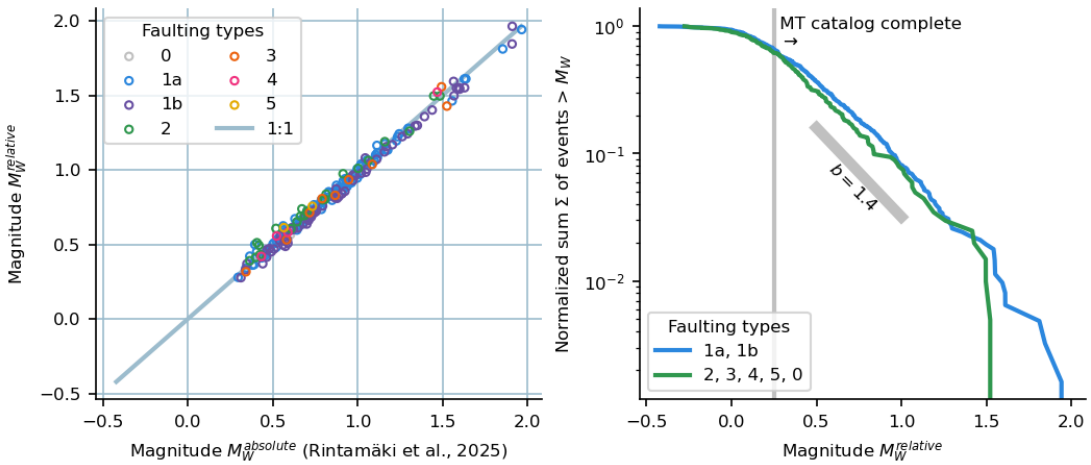


Figure 3. Magnitude distribution separated by faulting type. Left: Validation of magnitude estimates against absolute MTs (Rintamäki et al., 2025). Right: Normalized Gutenberg-Richter distribution. The data suggest that larger events are over-represented in group 1. See Fig. 2 and text for definition of faulting type groups.

4 CONCLUSION AND OUTLOOK

The relative moment tensor method has the ability to resolve the faulting mechanism of small earthquakes, even with limited knowledge of subsurface properties. It is especially suited to characterize induced seismicity, which typically is clustered and of low magnitude. Induced seismicity frequently satisfies the two main assumptions of the relative moment tensor method, namely a comparable Green's function between seismic events and an adequate description of a seismic event as a point source. The application of the method to stimulation seismicity of a 6.1 km deep geothermal well in gneiss and granite of the Fennoscandian Shield yields moment tensors down to a magnitude M_W of -0.5, complete above ca. M_W = 0.2. Moment tensors are of sufficient abundance to include them in statistical analysis.

With the present implementation *relMT* (Bloch et al., 2026), analysis is sufficiently easy and fast to be performed by an expert analyst within days or weeks. It can contribute to characterizing geothermal reservoirs in terms of structure and seismic potential, and potentially inform future stimulation operations. A prototype enhancement of the method removes the necessity to constrain the system of linear equations with an absolute moment tensor, but to only require a few P-wave first motion polarities across the data set (Drolet et al., 2023). Incorporation of the P-polarity constraint may facilitate computation of relative moment tensors in near real-time, appropriate for monitoring purposes.

Acknowledgements

Funded by the EU through a Marie Skłodowska-Curie fellowship to W.B. under Grant Agreement Nr. 101146483.

REFERENCES

Bloch, W, Plourde, A., Drolet, D., & Bostock, M. relMT: Software to compute relative seismic moment tensors (v0.4.0-beta) *Zenodo*. (2025) https://doi.org/10.5281/zenodo.18505641

Bostock, M., Plourde, A., Drolet, D., and Littel, G. Multichannel alignment of S waves. *Bulletin of the Seismological Society of America*, **112(1)**, (2022), 133-142.

Drolet, D., Bostock, M., and Peacock, S. Relative Moment Tensor Inversion for Microseismicity: Application to Clustered Earthquakes in the Cascadia Forearc. *Seismica*, ***2*(4)**, (2023)

Kwiatek, G., Saarno, T., Ader, T., Bluemle, F., Bohnhoff, M., Chendorain, M., Dresen, G., Heikkinen, P., Kukkonen, I., Leary, P. and Leonhardt, M., Malin, P., Martínez-Garzón, P., Passmore, K., Passmoe, P., Valenzuela, S., and Wollin, C. Controlling fluid-induced seismicity during a 6.1-km-deep geothermal stimulation in Finland. Science *Advances*, **5(5)**, (2019), eaav7224.

Leonhardt, M., Kwiatek, G., Martínez-Garzón, P., Bohnhoff, M., Saarno, T., Heikkinen, P., and Dresen, G. Seismicity during and after stimulation of a 6.1 km deep enhanced geothermal system in Helsinki, Finland. *Solid Eart*, **12**, (2021), 581-594.

Plourde, A. P., and Bostock, M. G. Relative moment tensors and deep Yakutat seismicity. *Geophysical Journal International*, **219(2**), (2019) 1447-1462.

Rintamäki, A. E., Hillers, G., Heimann, S., Dahm, T., and Korja, A. Centroid Full Moment Tensor Patterns of Induced M_W 0.3–2.0 Earthquakes in the Fennoscandian Shield. *Bulletin of the Seismological Society of America*, **115(3)**, (2025), 1352-1380.